Asian Journal of Information Tachnology 4 (11): 971-977, 2005

Characterization of Discrete Cosine Transform Based Generalized Gradient Vector Flow Active Contours for Boundary Mapping of Chromosome Spread Images and Investigations

[1]A.Prabhu Britto and [2]G.Ravindran
[1]Center for Medical Electronics, Department of Electronics and Communication Engineering,
[2]Chairman, Faculty of Information and Communication Engineering,Anna University, Chennai 600 025 India

Abstract: This study characterized and investigated optimality of Generalized gradient vector flow active contours as a suitable boundary mapping technique for Chromosome spread images having variability in shape and size. Boundary mapping using generalized gradient vector flow active contours is done on chromosome spread images and it is found that a unique set of parameter values for the technique is required for boundary mapping every chromosome image. Characterization studies have shown that an optimal range of values exists for each parameter within which good boundary mapping results can be obtained for various chromosomes in similar class of images. Statistical testing validates the experimental results.

Key words: Generalized gradient vector flow, active contour, deformable curve, chromosome, boundary mapping, characterization

INTRODUCTION

This study aims to obtain accurate segmentation results using Generalized gradient vector flow field active contours from chromosome spread images that have variable image properties. The various parameters in the chosen active contour formulation are investigated for an optimal selection. Noise and artifacts can possibly cause incorrect segmentation or boundary discontinuities in segmented objects[1].

ACTIVE CONTOUR MODELS

Active contours also called as Snakes or Deformable Curves, first proposed by Kass[2] are energy-minimizing contours that apply information about the boundaries as part of an optimization procedure. They are generally initialized around the object of interest by automatic or manual process. The contour then deforms itself iteratively from its initial position in conformity with nearest dominant edge feature by minimizing the energy composed of the Internal and External forces, thus making the model active. The energy minimization process can be viewed as a dynamic problem where the active contour model is governed by the laws of elasticity and lagrangian dynamics[3], and the model evolves until equilibrium of all forces is reached.

FORMULATION OF ACTIVE CONTOUR MODELS

An Active Contour Model can be represented by a curve c, as a function of its arc length τ, $c(\tau) = \left(\frac{x(\tau)}{y(\tau)}\right)$ -- (1) with $\tau = [0 \ldots 1]$. To define a closed curve c(0) is set to equal c(1). A discrete model can be expressed as an ordered set of n vertices $v_i = (x_i, y_i)^T$ with $v=(v_1,\ldots,v_n)$. The large number of vertices required to achieve accuracy could lead to high computational complexity and numerical instability [3]. Mathematically, an active contour model can be defined in discrete form as a curve x(s)=[x (s),y (s)],s ε[0,1]that moves through the spatial domain of an image to minimize the energy

$$E = \int_0^1 \frac{1}{2} \left(\alpha \left|X'(s)\right|^2 + \beta \left|x''(s)\right|^2\right) + E_{ext}(x(s))ds \quad (2)$$

functional where, α and β are weighting parameters that control the active contour's tension and rigidity, respectively[4]. The first order derivative discourages stretching and the second order derivative discourages bending. á and â govern the effect of the derivatives on the snake. The external energy function E_{ext} is derived from the image so that it takes on its smaller values at the features of interest such as boundaries and guides the active contour towards the boundaries.

$$E_{ext} = K\left|G_\sigma(x,y) * I(x,y)\right| \quad (3)$$

The external energy is defined by where, $G_ó(x,y)$ is a two-dimensional Gaussian function with standard deviation ó, I(x,y) represents the image, and ê is the external force weight. This external energy is specified for a line drawing (black on white) and positive ê is used. A motivation for applying some Gaussian filtering to the underlying image is to reduce noise.

Corresponding Author: A.Prabhu Britto,Center for Medical Electronics, Dept. of Electronics and Communication Engineering, Anna University, Chennai 600 025 India

An active contour that minimizes E must satisfy the Euler Equation

$$\alpha x''(s) - \beta x''''(s) - \nabla E_{ext} = 0 \quad (4)$$

where $F_{int} = \alpha x''(s) - \beta x''''(s)$ And $F_{ext} = -\nabla E_{ext}$ comprise the components of a force balance equation such that

$$F_{int} + F_{ext} = 0 \quad (5).$$

The internal force F_{int} discourages stretching and bending while the external potential force F_{ext} drives the active contour towards the desired image boundary. Eq. 4 is solved by making the active contour dynamic by treating x as a function of time t as well as s. Then the partial derivative of x with respect to t is then set equal to the left hand side of Eq. 4 as follows

$$x_t(s,t) = \alpha x'''(s,t) - \nabla E_{ext} \quad (6)$$

A solution to Eq. 6 can be obtained by discretizing the equation and solving the discrete system iteratively[2]. When the solution x (s,t) stabiiizes, the term x_t (s,t) vanishes and a solution of Eq. 4 is achieved.

Traditional active contour models suffer from a few drawbacks. Boundary concavities leave the contour split across the boundary. Capture range is also limited. Methods suggested to overcome these difficulties, namely multiresolution methods[5], pressure forces[6], distance potentials[7], control points[8], domain adaptivity[9], directional attractions[10] and solenoidal fields[11], however solved one problem but introduced new ones[12]. Hence, this new class of external fields called gradient vector flow fields[12,13] was suggested to overcome the difficulties in traditional active contour models.

GRADIENT VECTOR FLOW (GVF) ACTIVE CONTOURS

Gradient Vector Flow (GVF) active contours use gradient vector flow fields obtained by solving a vector diffusion equation that diffuses the gradient vectors of a gray-level edge map computed from the image. The GVF active contour model cannot be written as the negative gradient of a potential function. Hence it is directly specified from a dynamic force equation. The external forces arising out of GVF fields are non-conservative forces as they cannot be written as gradients of scalar potential functions and they show improved performance compared to traditional energy-minimizing active contours[12, 13].

The GVF field points towards the object boundary when very near to the boundary, but varies smoothly over homogeneous image regions extending to the image border. Hence the GVF field can capture an active contour from long range from either side of the object boundary and can force it into the object boundary. The gradient vectors are normal to the boundary surface but by combining Laplacian and Gradient the result is not the normal vectors to the boundary surface. As a result of this, the GVF field yields vectors that point into boundary concavities so that the active contour is driven through the concavities. Information regarding whether the initial contour should expand or contract need not be given to the GVF active contour model. The GVF active contour model has a large capture range. The GVF is very useful when there are boundary gaps, because it preserves the perceptual edge property of active contours[2, 13]. Also, the GVF provides for flexible initialization of the initial contour. This GVF field is defined as the equilibrium solution to the following vector diffusion equation[12],

$$u_t = g(|\nabla f|)\ \nabla^2 u - h(|\nabla f|)(u - \nabla f) \quad (7a)$$

and

$$u(x,0) = \nabla f(x) \quad (7b)$$

where, u_t denotes the partial derivative of u(x,t) with respect to t, ∇^2 is the Laplacian operator (applied to each spatial component of u separately), and f is an edge map that has a higher value at the desired object boundary. The functions in g and h control the amount of diffusion in GVF. In Eq.7, $g(|\nabla f|)\ \nabla^2 u$ produces a smoothly varying vector field, and hence called as the smoothing term, while $h(|\nabla f|)(u - \nabla f)$ encourages the vector field u to be close to ∇f computed from the image data and hence called as the data term. The weighting functions g (.)and h (.)apply to the smoothing and data terms respectively and they are chosen as $g(|\nabla f|) = \mu$ and $h(|\nabla f|) = |\nabla f|^2$ [13]. g(.) is constant here, and smoothing occurs everywhere, while h(.)grows larger near strong edges and dominates at boundaries. Hence, the gradient vector flow field is defined as the vector field v (x,y) =[u(x,y),v (x,y)] that minimizes the energy functional

$$\varepsilon = \iint \mu\left(u_x^2 + u_y^2 + v_x^2 + v_y^2\right) + |\nabla f|^2 |v - \nabla f|^2 \, dxa \quad (8)$$

The effect of this variational formulation is that the result is made smooth when there is no data. When the gradient of the edge map is large, it keeps the external field nearly equal to the gradient, but keeps field to be slowly varying in homogeneous regions where the gradient of the edge map is small, i.e., the gradient of an edge map ∇f

has vectors point toward the edges, which are normal to the edges at the edges, and have magnitudes only in the immediate vicinity of the edges, and in homogeneous regions ∇f is nearly zero. μ is a regularization parameter that governs the tradeoff between the first and the second term in the integrand in Eq. 8. The solution of Eq. 8 can be done using the Calculus of Variations and further by treating u and v as functions of time, solving them as generalized diffusion equations[13].

GENERALIZED GRADIENT VECTOR FLOW (GGVF) ACTIVE CONTOURS

In the GVF Active Contour formulation given by Eq. 7, the term $g(\nabla f)$ is constant and hence smoothing occurs everywhere, whileh(∇f) grows larger near strong edges, dominating at boundaries. However when there are two edges in close proximity, it manifests as a long, thin indentation along the boundary. This makes the GVF tend to smooth between opposite edges. Hence the GVF loses forces to drive the Active Contour into this region.

Xu and prince[14] proposed suitable weighting functions in which g(.) becomes smaller as h(.) becomes larger. Therefore there will be very little smoothing in the proximity of large gradients. Hence the effect vector field will be nearly equal to the gradient of the edge map. There are many ways to specify these pairs of weighting functions, thus making the formulation a Generalized Gradient Vector Active Contour formulation. Xu and prince[14] the following weighting functions were

$$g(|\nabla f|) = e^{-\left(\frac{|\nabla f|}{k}\right)^2} \tag{9}$$

and

$$h(|\nabla f|) = 1 - g(|\nabla f|) \tag{10}$$

This choice of weighting functions will make the computed GGVF field to conform to the edge map gradient at strong edges, but will vary smoothly away from boundaries. The solution remains the same as discussed in GVF Active Contours in the preceding paragraphs.

DISCRETE COSINE TRANSFORM (DCT) BASED GGVF ACTIVE CONTOURS

Transform theory plays a fundamental role in image processing. The transform of an Image yields more insight into the properties of the image. The Discrete Cosine Transform has excellent energy compaction. Hence, the Discrete Cosine Transform promises better description of the image properties. Therefore, the Discrete Cosine Transform is embedded into the boundary mapping scheme to obtain better energy compaction. The 2D DCT is defined as:

$$C(u,v) = \alpha(u)\alpha(v)\sum_{x=0}^{N-1}\sum_{y=0}^{N-1} f(x,y)\cos\left[\frac{(-2x+1)u\lambda}{2N}\right]\cos\left[\frac{(-2Y+1)V\lambda}{2N}\right]$$

$$\cos\left[\frac{(-2y+1)v\pi}{2N}\right] \tag{11}.$$

The local contrast of the Image at the given pixel location (k,l) is given by

$$P(k,l) = \frac{\sum_{t=1}^{2(2n+1)-1} w_t E_t}{d_{00}} \tag{12}$$

where:

$$E_t = \frac{\sum_{u+v=t} |d_{u,v}|}{N} \tag{13}$$

and:

$$N = \begin{cases} t+1 & t < 2n+1 \\ 2(2n+1)-t & t \geq 2n+1 \end{cases} \tag{14}.$$

Here, w_t denotes the weights used to select the DCT coefficients. The local contrast P(k,l) is then used to generate a DCT contrast enhanced Image[15], which is then subject to selective segmentation by the energy compact gradient vector flow active contour model using Eq. 8.

RESULTS AND DISCUSSION

The chromosome metaphase image (size 480x512 pixels at 72 pixels per inch resolution) was taken and preprocessed. Insignificant and unnecessary regions in the image were removed interactively. The chromosome of interest was selected by user selection of a few points on the chromosome spread image that formed the vertices of a polygon. On constructing the perimeter of the polygon from the selection points, seed points for the initial contour were determined automatically by periodically selecting every third pixel along the perimeter of the polygon. The GGVF deformable curve was then allowed to deform until it converged to the chromosome boundary. The optimum parameters for the deformable curve with respect to the Chromosome images were determined by tabulated studies. The image was made to undergo minimal preprocessing. The DCT based GGVF Active contour is governed by the following parameters, namely, ó, μ, á, â and ê. ó determines the Gaussian filtering that is applied to the image to generate the external field. Larger value of ó will cause the boundaries to become blurry and distorted, and can also cause a shift

in the boundary location. However, large values of ó are necessary to increase the capture range of the active contour. μ is a regularization parameter in Eq. (8), and requires a higher value in the presence of noise in the image. á determines the tension of the active contour and â determines the rigidity of the contour. The tension keeps the active contour contracted and the rigidity keeps it smooth. á and â may also take on value zero implying that the influence of the respective tension and rigidity terms in the diffusion equation is low. ê is the external force weight that determines the strength of the external field that is applied. The iterations were set suitably.

Experimental Results: A few chromosome samples, their corresponding DCT based GGVF fields, and their output samples are presented here.

The Figs. 1-6 shows original chromosome image samples, their corresponding DCT based GGVF fields and boundary mapped chromosome images as output images. For example, Fig. 1a shows an original chromosome sample, Fig. 1b shows its corresponding DCT based GGVF field and Fig. 1c shows the corresponding boundary mapped output image.

The graphical outputs show successful boundary mapping of chromosome images using DCT based GGVF Active Contours.

Experimental Validation: In this work, ground truth model is not available and hence validation is performed on ordinal or ranking scale and then quantified. A set of 20 random samples is taken and characterization of each parameter is done. The outputs were tabulated in ranking order with "1" describing the best quality output and as the quality decreases the rank increases up to rank "97". Rank "98" is a special case, where the output image is rejected based on quality or the output image is not available due to numerical instability possibly caused due to the greater number of contour points[3]. The tables represent characterization studies for each parameter.Since, each table denotes variation for only one parameter either between the lower and upper limits of the parameter or between the lower and upper limits giving significantly different output, with the other parameters taking a constant value, the best parameter value of that table is the one that gives maximum good quality outputs for all samples or a majority of samples. The statistical median is used to judge the distribution of values for each parameter value for all samples. An important point to be noted is that characterization studies have been performed for those parameter values which give either significant output or significant difference in performance between adjacent parameter values. Those parameter values where there is no significant difference between adjacent parameter values have not been tabulated. Also, those parameter values outside the tabulated range which gave no proper results have not been tabulated.

Table.1 Characterization of Sigma Hence the optimal set of parameter values that give good boundary mapping for

Fig. 1a Sample

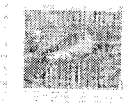

Fig. 1b: DCT GGVF

Fig. 1c Output

Fig. 2a Sample 2

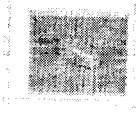

Fig. 2b DCT GGVF

Fig. 2c Output

Fig. 3a Sample 3

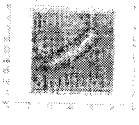

Fig. 3b DCT GGVF

Fig. 3c Output

Fig. 4a Sample 4

Fig. 4b DCT GGVF

Fig. 4c Output

Fig. 5a Sample 5

Fig. 5b DCT GGVF

Fig. 5c Output

Fig. 6a Sample 6

Fig. 6b DCT GGVF

Fig. 6c Output

the given class of chromosome images is ó = 4, μ = 0.01, á = 0.1, â = 0.1, and ê = 0.5. A safe limit of 5% tolerance can be introduced to the optimal range of parameter values to make them suitable for use in similar classes of chromosome spread images as shown in Table 6.

Statistical validation: In each characterization table, only that parameter varies, while other parameters take on constant values. Hence one way Anova is very suitable to validate the experimental results.

Table.1:Characterization of Sigma

	DCT GGVF				
Sample No	0.50	1.00	2.00	4.00	6.00
1	97	77	30	5	77
2	97	77	30	5	29
3	97	77	30	5	57
4	97	71	71	7	32
5	97	86	86	97	58
6	86	86	86	38	48
7	86	86	86	34	86
8	86	86	86	38	38
9	79	79	30	21	31
10	79	29	29	29	29
11	79	77	30	38	31
12	86	86	86	82	97
13	86	86	86	50	97
14	78	86	60	60	29
15	77	86	30	30	75
16	78	78	86	5	31
17	78	78	78	16	31
18	77	77	67	13	25
19	77	79	30	21	64
20	86	86	77	38	47
median	86	79	69	29	43

In Table 1, the median indicates that the acceptable optimal range of ó is restricted to the value 4. The best value compared qualitatively amongst those tested is 4 and hence it is chosen for performing further characterization.

Table 2: Characterization of Mu

	DCT GGVF		
Sample No	0.005	0.014	0.1
1	21	5	97
2	5	5	97
3	5	5	97
4	23	7	97
5	97	97	97
6	40	38	44
7	50	34	33
8	50	38	33
9	23	21	35
10	23	29	97
11	46	38	97
12	97	82	33
13	97	50	97
14	75	30	33
15	78	30	97
16	21	5	97
17	40	16	97
18	19	13	97
19	31	21	97
20	46	38	33
Median	40	29	97

The median indicates that the acceptable optimal range of μ is restricted to the value 0.01. The best value compared qualitatively amongst those tested is 0.01 and hence it is chosen for performing further characterization.

At the customary 0.05 significance level, one way Anova test yields a p-value of 2.2905E-12 on Table1. The very small p value indicates that the differences between the column means are highly significant. This impliesthat the results inTable 1 are significant and hence a clear distinction is made using the median value

Table 3:Characterization of Alpha

	DCT GGVF		
sample No	0.01	0.1	0.2
1	5	5	21
2	5	5	19
3	5	5	21
4	7	5	16
5	97	97	97
6	38	38	46
7	34	50	50
8	38	38	54
9	21	21	21
10	29	8	21
11	38	38	46
12	82	38	97
13	50	54	94
14	30	34	78
15	30	46	21
16	5	5	38
17	16	16	40
18	13	5	29
19	21	40	40
20	38	46	46
Median	29	36	40

The median indicates that the acceptable optimal range of á extends from 0.01 to 0.2. The best value compared qualitatively amongst those tested is 0.1 and hence it is chosen for performing further characterization.

Table 4:Characterization of Beta

	DCT GGVF		
Sample No	0.02	0.0	0.2
1	5	5	21
2	5	5	21
3	5	5	21
4	5	5	70
5	97	97	97
6	38	48	46
7	50	43	34
8	38	46	86
9	21	7	21
10	7	7	21
11	38	13	78
12	38	97	82
13	54	54	57
14	34	13	46
15	46	46	34
16	5	5	5
17	16	16	46
18	5	5	21
19	40	21	21
20	46	13	38
Median	36	13	36

The median indicates that the acceptable optimal range of â extends from 0.02 to 0.2. The best value compared qualitatively amongst those tested is 0.1 and hence it is chosen for performing further characterization.

for choosing suitable value of parameter sigma. In Table 2, one way Anova test yields a p-value of 2.40817E-05 at the 0.05significance level. This implies that the results in Table2 are significant and hence a clear distinction is made using the median value for choosing suitable value of parameter mu.

Table 5: Characterization of Kappa

	DCT GGVF		
Samle No	0.4	0.5	0.6
1	21	5	21
2	5	5	5
3	5	5	21
4	70	5	5
5	97	97	97
6	47	48	46
7	50	43	38
8	54	46	38
9	21	7	30
10	30	7	21
11	30	13	21
12	97	97	97
13	50	54	97
14	30	13	30
15	50	46	50
16	30	5	5
17	16	16	38
18	21	5	21
19	21	21	21
20	30	13	38
Median	30	13	30

The median indicates that the acceptable optimal range of ê extends from 0.4 to 0.6. The best value compared qualitatively amongst those tested is 0.5.

Table 6: Optimal range of DCT based GGVF active contour parameter values for chromosome spread images (based on experimental validation)

Parameter	Parameter values used for tested spread image	Acceptable range of Parameter values	Acceptable range of values at 5% tolerance
DCT GGVF Sigma	4	(4)	(3.8000 , 4.2000)
DCT GGVF Mu	0.01	(0.01)	(0.0095 , 0.0105)
DCT GGVF Alpha	0.1	(0.01 to 0.2)	(0.0095 , 0.2100)
DCT GGVF Beta	0.1	(0.02 to 0.2)	(0.0190 , 0.2100)
DCT GGVF Kappa	0.5	(0.4 to 0.6)	(0.3800 , 0.6300)

In Table 3, one way Anova test yields a p-value of 0.1069 at the 0.05significance level. Therefore, the entire range of parameter values tabulated is selected as the optimal range for the parameter alpha. In Table 4, at the 0.05 significance level one way ANOVA yields a p-value of 0.139. Therefore, the entire range of parameter values tabulated is selected as the optimal range for the parameter beta. In Table5, at the 0.05 significance level, one way Anova yields a p-value of 0.4071. Therefore, the entire range of parameter values tabulated is selected as the optimal range for the parameter kappa (Table 5).

Validation of Robustness of the Boundary Mapping Scheme: The following difficulties were observed during the implementation of the boundary mapping scheme. The banding pattern present in the chromosomes gives rise to higher contrast compared to the outer edges, which causes the DCT based GGVF external field to have a higher strength at the bands. Therefore, the DCT based GGVF Active Contour feels more attraction towards the bands than the outer boundary.

The chromosome images in the chromosome spread image have variability in shape and size due to the nature of the spread image. Also, the spatial distribution of the chromosomes is random accompanied by uneven spacing between adjacent chromosomes. Hence, each chromosome in a chromosome spread image becomes a unique sample. There is also a need for unique number of iterations to converge. The small object size of the chromosomes makes the computed DCT based GGVF field also to be small. Hence suitable choice of parameters is necessary. The chromosomes in the spread image have a minor axis length varying between 14 and 17 pixels approximately and major axis length varying between 30 and 80 pixels approximately at 72 pixels per inch resolution. This causes the DCT based GGVF external field to have a high density at corners. Accompanied with the banding characteristic, the axis lengths force the DCT based GGVF Active Contour to map contours at the inner region of the chromosome instead of the actual boundary at the periphery of the chromosome. The weak edges in chromosomes also contribute to the Active Contour to overwhelm weak edges and move into inner regions. These difficulties make the task of boundary mapping of chromosomes in chromosome spread images very difficult. Experimental Validations prove that the boundary mapping has been very successful. Hence the robustness of the scheme is thus validated.

CONCLUSIONS

The DCT based GGVF Active Contour establishes itself as a very good universal boundary mapping technique for chromosome spread images having chromosomes with variable shape and variable image properties.

ACKNOWLEDGEMENTS

The authors wish to thank Prof. Ken Castleman and Prof. Qiang Wu, both from Advanced Digital Imaging Research, Texas for their help in providing chromosome images.

REFERENCES

1. McInerney, T. and D. Terzopoulos 1996. Deformable models in medical image analysis , IEEE Proceedings of the Workshop on Mathematical Methods in Biomedical Image Analysis, pp: 171-180.
2. Kass, M., A. Witkin and D. Terzopoulos, 1987. Snakes: Active contour models , Intl. J. Comp. Vision 1: 321-331.
3. Rueckert, D., 1997. Segmentation and tracking in cardiovascular MR images using geometrically deformable models and templates , Ph.D Thesis, Imperial College of Science, Technology and Medicine, London.
4. Xu, C. and J.L. Prince, 1997. Gradient Vector Flow: A new external force for snakes , IEEE Proc. Conf. on Comp. Vis. Patt. Recog. (CVPR'97), pp: 66-71
5. Leroy, B., I. Herlin and L.D. Cohen, 1996. Multi-resolution algorithms for active contour models. In: 12th Intl. Conf. on Analysis and Optimization of Systems, pp: 58-65.
6. Cohen, L.D., 1991. On active contours and balloons .CVGIP: Image Understanding, 53: 211-218.
7. Cohen, L.D. and I. Cohen, 1993 Finite-element methods for active contour models and balloons for 2-D and 3-D images , IEEE Trans. On Pattern Anal. Machine Intell., 15(11):1131-1147.
8. Davatzikos, C. and J.L. Prince, 1995. An active contour model for mapping the cortex . IEEE Trans. Medical Imaging, 14: 65-80.
9. Davatzikos, C. and J.L. Prince, 1994. Convexity analysis of active contour models , In Proc. Conf. Info. Sci. Sys., pp: 581-587.
10. Abrantes, A.J., and J.S. Marques, 1996. A class of constrained clustering algorithms for object boundary extraction, IEEE Trans. Image Processing, 5: 1507-1521.
11. Prince, J.L. and C. Xu, 1996 A new external force model for snakes , In 1996 Image and Multidimensional Signal Processing Workshop, pp:30-31.
12. Xu, C. and J.L. Prince, 2000. Gradient Vector Flow Deformable Models, In: Handbook of Medical Imaging, Academic Press, pp:159-170
13. Xu, C. and J.L. Prince, 1998. Snakes, shapes and gradient vector flow, IEEE Trans. Image Processing, 7: 359-369.
14. Xu, C. and J.L. Prince, 1998. Generalized gradient vector flow external forces for active contours, Signal Processing, 71: 131 – 139.